Title

VIBRATIONAL AND ELECTRONIC SPECTROSCOPY OF PYRIDINE AND BENZENE ADSORBED ON THE Rh(lll) CRYSTAL FURFACE

Author

Mate, CM.

Publication Date

1987-07-01

LBL-23628
Preprint

Lawrence Berkeley Laboratory
UNIVERSITY OF CALIFORNIA

Materials & Chemical Sciences Division

Submitted to Journal of Chemical Physics

Vibrational and Electronic Spectroscopy of Pyridine and Benzene Adsorbed on the Rh(111) Crystal Surface

C.M. Mate, G.A. Somorjai,
H.W.K. Tom, X.D. Zhu, and Y.R. Shen

July 1987

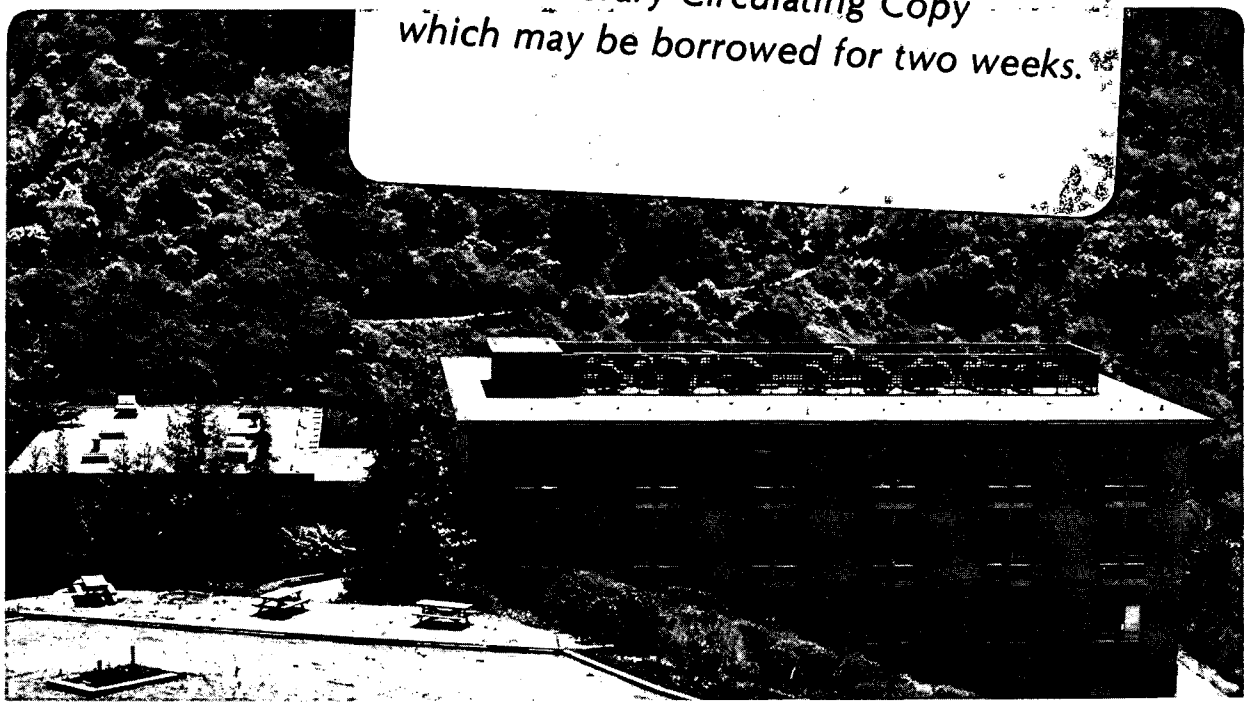

Prepared for the U.S. Department of Energy under Contract DE-AC03-76SF00098

DISCLAIMER

LBL-23628

VIBRATIONAL AND ELECTRONIC SPECTROSCOPY OF PYRIDINE AND BENZENE ADSORBED ON THE Rh(111) CRYSTAL SURFACE

C.M. Mate[a] and G.A. Somorjai

Materials and Chemical Sciences Division, Lawrence Berkeley Laboratory

Department of Chemistry, University of California

Berkeley, California 94720, USA

H.W.K. Tom[b], X.D. Zhu and Y.R. Shen

Materials and Chemical Sciences Division, Lawrence Berkeley Laboratory

Department of Physics, University of California

Berkeley, California 94720, USA

(a) Also affiliated with Department of Physics, University of California, Berkeley, CA 94720, USA; present address: IBM Almaden Research Center, San Jose, CA 95120, USA.

(b) Permanent address: AT&T Bell Laboratories, Holmdel, New Jersey 07760, USA

ABSTRACT

We report the vibrational and electronic spectra for pyridine and benzene adsorbed on the Rh(111) crystal surface obtained by high-resolution electron energy loss spectroscopy (HREELS). Low energy electron diffraction (LEED), thermal desorption spectroscopy (TDS), and optical second harmonic generation (SHG) have also been used to provide complementary information. Pyridine adsorption on Rh(111) was studied over the 77 to 450 K temperature range. At 77 K, multilayers of pyridine are observed with a vibrational spectrum similar to that of liquid pyridine. Between 185 to 230 K, HREELS and TDS indicate that both physisorbed and chemisorbed pyridine species are present on the surface. The physisorbed species desorbs at 295 K, while the chemisorbed species is stable until it decomposes on the surface at 400 K. We propose that the chemisorbed species is an α-pyridyl complex as thermal desorption spectroscopy indicates partial dehydrogenation of this pyridine surface species. Electronic energy loss spectra for both benzene and pyridine adsorbed at 310 K show only a weak transition centered at ~4eV. The absence of prominent $\pi \rightarrow \pi^*$ transitions, which are readily observed for multilayers of benzene adsorbed on Rh(111), implies that the π orbitals are strongly involved in the chemisorption bond of these molecules with the Rh(111) surface.

1. INTRODUCTION

The interaction of aromatic molecules with metal surfaces has recently been the subject of several investigations [1-33]. Much of this interest is derived from the importance of aromatic molecules as fuels, chemicals, and lubricants that are produced and utilized by technologies where surface phenomena play a dominant role. For example, aromatic compounds are desirable products of heterogeneous catalytic reactions in the refining of crude oil into high octane fuels [34]. In lubrication, aromatic compounds are frequently used as functional groups in extreme pressure additives [35], even though their role is not understood. Therefore, a molecular scale understanding of how aromatic molecules interact with metal surfaces should be of considerable importance.

In this work, we have studied pyridine and benzene, two of the simplest aromatic molecules, adsorbed on the Rh(111) crystal surface using high-resolution electron energy loss spectroscopy (HREELS), low energy electron diffraction (LEED), thermal desorption spectroscopy (TDS), and second harmonic generation (SHG). Here, HREELS is used for both vibrational and electronic spectroscopy and provides the bulk of the information concerning the atomic and electronic structure of these adsorbates, while LEED, TDS, and SHG provide useful complementary information about the ordering and bonding of these molecules to the surface.

For pyridine multilayers adsorbed on Rh(111) at 77K, our vibrational spectra indicate that pyridine is unperturbed from that in the liquid state. After annealing the Rh sample to 185 K so as to remove the pyridine multilayers, the vibrational spectra indicate that both a chemisorbed and physisorbed pyridine species are present on the surface. The physisorbed

pyridine species is observed to desorb in TDS at 295 K leaving the chemisorbed pyridine species, which is stable on the surface up to 400 K. As TDS also indicates that some pyridine dehydrogenation occurs at temperatures below 250 K, we propose that the chemisorbed pyridine species is an α-pyridyl species (i.e., a pyridine molecule that has lost an α-hydrogen atom).

Pyridine has also been extensively studied on several other metal surfaces; Figure 1 summarizes the reaction of pyridine with these surfaces - Pt(111), Pt(110), Ni(100), Ag(111), Pd(111), Ir(111) and Cu(110) - as well as the reaction with the Rh(111) surface. The nitrogen atom of pyridine can participate in some interesting chemistry when the molecule adsorbs on a surface. First, there can be competition between the electrons in the nitrogen lone-pair and the π-orbitals as to which will be dominantly responsible for the pyridine-metal bond. Such competition, where the molecule converts from a relatively flat lying, π-bonded species to a tilted, nitrogen-bonded species with increasing coverage, has been observed by HREELS and NEXAFS for pyridine adsorbed on the Ag(111) surface at 100K [11,22] and by HREELS for pyridine adsorbed on the Ni(100) surface at 170 K [12] and on Pt(110) at 310 K [33] (the conversion takes place at 0.7 of a pyridine monolayer on Ag(111)[22]). Second, pyridine has also been observed to lose one of the α-hydrogens on several other metal surfaces (Pt(111)[13,21], Ni(100)[12,27]) above a particular temperature (~300 K on both Pt(111) and Ni(100)) to form an α-pyridyl species. Pyridine adsorption has also been recently studied by HREELS on the Pd(111) surface [14,15] where the molecule was determined to adsorb as a relatively flat lying, π-bonded species at low temperatures (150 K $<T<$ 300 K); but two different results have been obtained

for pyridine adsorbed at 300 K on Pd(111), with Grassian and Muetterties [14] observing a tilted, nitrogen bonded species and Waddill and Kesmodel [15] observing a flat lying, π-bonded species. A nitrogen bonded pyridine species on Pd(111) at 300 K, though, is consistent with angle resolved ultraviolet photoemission (ARUPS) results of Netzer and Mack [19,25]. A tilted pyridine species has also been observed by ARUPS for pyridine adsorbed on Ir(111)[24] and Cu(110)[23] at room temperature.

Benzene adsorption has been investigated more extensively than pyridine and so far has been studied on Ag(111)[17], Ir(111)[24], Ni(111)[18,29,30,31], Ni(110)[30], Ni(100)[29], Rh(111)[1-10], Pd(111)[12,14,19,28], Pd(100)[28], Pt(111)[5,26,31], Pt(110)[33], Pt_{50} Ni_{50} (111)[32], $Pt_{78}Ni_{22}$(111)[32] surfaces. Generally, benzene has been found to bond with its molecular ring parallel to the surface and to form the adsorption bond through its π-orbitals.

For benzene adsorption on Rh(111), our results obtained by vibrational spectroscopy, LEED, and TDS are the same as those previously reported [1-7] and are only briefly discussed here. The new results presented here for benzene adsorption on Rh(111) concern the electronic structure of the adsorbed benzene, which we also present for adsorbed pyridine. In the electronic energy loss spectra for both benzene and pyridine adsorbed at 310 K, only a weak transition centered at ~4eV is observed and is interpreted as either a charge transfer excitation or weak $\pi \rightarrow \pi^*$ transitions. The absence of the prominent $\pi \rightarrow \pi^*$ transitions, which are readily observed for multilayers of benzene adsorbed on the Rh(111) surface, implies that the π orbitals are strongly involved in the chemisorption bond.

2. Experimental

Our experiments were conducted in a two level ultra-high vacuum system with an HREEL spectrometer occupying the lower level, while LEED, Auger-electron spectroscopy, TDS and SHG experiments were performed on the upper level. The Rh(111) surface was cleaned with cycles of Ar^+ sputtering, heating at 1000 K in $2x10^{-7}$ torr of O_2, annealing at 1200 K in vacuum, and then flash heating to 1300 K. Surface cleanliness was monitored by Auger-electron spectroscopy and HREELS. During experiments the background pressure in the chamber was typically $1x10^{-10}$ torr.

Our HREEL spectrometer is similar to designs commonly used [36] and consists of 127° cylindrical monochromator and analyzer sectors. The spectrometer has a rotatable analyzer and was operated with $\theta_{in} = \theta_{out} = 65°$ from the surface normal. For the vibrational spectra, the spectrometer was operated at an overall system resolution between 7 and 7.5 meV (55 and 60 cm^{-1}) and with an incident beam energy between 4 and 6 eV. For the electronic energy loss spectra, the resolution was 15 meV and the incident beam energy was near 20 eV.

For the optical second-harmonic experiments, Nd:YAG laser pluses at 1.06 or 0.532 μm with ~ 7 ns pulsewidth and 6 mJ pulse energy were p-polarized and incident on the Rh(111) sample at an angle of 67.5° with a beam diameter of 1 mm. At this intensity, no laser-induced desorption or surface damage could be detected. The SH radiation from the surface was detected, after proper filtering, by a photomultiplier in conjunction with a gated integrator system. The SH signal generated from the clean surface was fairly strong, about 10^3 photons/pulse.

3. Results and Discussion

3.1 Pyridine Adsorption on Rh(111)

3.1.1 Thermal Desorption Spectra (TDS)

The upper part of Figure 2 shows the thermal desorption spectrum for molecular desorption of NC_5H_5 following ~50 L exposure at 80 K, an amount sufficient to form multilayers of pyridine on the Rh(111) surface. The intense peak at 165 K results from the desorption of the pyridine multilayers, while the smaller peak at 295 K results from molecular pyridine desorbing from the pyridine monolayer in contact with the surface. Assuming first-order kinetics and a pre-exponential factor of 10^{13} sec^{-1}, the desorption energy is calculated from Redhead's equation [37] to be 9.7 kcal/mole for multilayer desorption in reasonable agreement with 9.0 kcal/mole for the heat of vaporization of pyridine measured at 347 K [38]. Also, the 295 K peak would then correspond to a desorption energy of 17.4 kcal/mole for molecular pyridine desorption for pyridine in contact with the surface, suggesting that the pyridine-surface bond is appreciably stronger than the pyridine-pyridine bond in the multilayer.

The lower part of Figure 2 shows the thermal desorption spectrum for D_2 desorption following the same exposure of NC_5D_5 at 80 K as used for the NC_5D_5 TDS. The first D_2 desorption peak occurs at a temperature (330 K) that is characteristic of hydrogen and deuterium desorption from the bare Rh(111) surface [39], suggesting that pyridine decomposition starts at temperatures below the onset of the 330 K desorption peak (i.e., below 250 K).

While the exact nature of the higher temperature desorption peaks in the D_2 desorption spectrum is not understood, they are fairly similar to the deuterium desorption peaks observed for benzene decomposition on Rh(111) [7],

with the 525 and 680 K peaks being more pronounced in the pyridine spectrum. Benzene is proposed to decompose on Rh(111) at 400 K into a mixture of C_xH fragments, which polymerize with increasing temperature. As discussed below, our HREELS results suggest perhaps similar thermal decomposition pathways occur for pyridine at 400 K on Rh(111) which accounts for the similarity in the D_2 desorption spectra.

3.1.2 HREELS of Pyridine/Rh(111)- Temperature Dependence

Figure 3a shows the the HREEL spectrum recorded in the specular direction at 77 K for multilayers of pyridine on the Rh(111) surface. The pyridine exposure was the same as that used for the thermal desorption experiments discussed above. For the multilayer coverages of pyridine, the HREEL spectrum is characterized by an elastic peak which is weak (1200 cps) and substantially broader (105 cm^{-1}) than the instrumental resolution of 60 cm^{-1}. When a HREEL spectrum was recorded at ten degrees away from the specular scattering direction, the peak intensities were virtually the same as the specular spectrum shown in Fig. 3a, implying that the predominant scattering mechanism is impact scattering [40]. We attribute the relatively strong impact scattering for the pyridine multilayer to possibly a resonance electron scattering effect that is also observed in gas phase pyridine [41].

Our assignment of the observed HREELS frequencies for the pyridine multilayer spectrum to the corresponding vibrational frequencies of liquid pyridine is given in Table 1 along with the mode number and symmetry representation of the liquid phase vibrational modes. Generally, the observed HREELS frequencies have been assigned to more than one pyridine vibrational mode, since the poor resolution makes it impossible to separate out vibrations

close in frequency. The HREELS frequencies for the pyridine multilayer do not appear to differ substantially from those of liquid pyridine, leading us to conclude that the pyridine in the multilayers is similar to that in the liquid phase, as expected.

Figure 3b shows the HREEL spectrum obtained in the specular direction at 77 K after the pyridine multilayer has been heated to 185 K. Heating to 185 K removes the pyridine multilayer but does not remove the second pyridine molecular desorption peak. In this spectrum, the elastic peak has narrowed to the instrumental resolution of 60 cm^{-1} and has increased in intensity to 2.7×10^4 cps. For spectra taken off specular, the 345, 465, 650, and 840 cm^{-1} features decrease in intensity implying that dipole scattering predominates for these features[40]. Since the 345, 465, 650, and 840 cm^{-1} features have the same frequencies and scattering mechanism as the vibrations of the chemisorbed pyridine species observed at 310 K, we assign these features to the same chemisorbed pyridine species also being present at 185 K. (We will defer discussion of the chemisorbed pyridine species until the following section where this species will be identified as an α-pyridyl species.)

The remaining HREELS features (at 770, 1025, 1240, 1450, 1590, and 3060 cm^{-1}) in Fig. 3b have similar intensities off specular as on specular, implying that impact scattering dominates for these features. Since these peaks have similar frequencies and absolute intensities, as well as the same scattering mechanism, as those observed for the pyridine multilayer spectrum, we assign them to a more weakly bound, physisorbed pyridine species that is coadsorbed with the chemisorbed species at 185 K. Since impact scattering dominates for the features of the physisorbed species, we are unable to use the dipole selection rule to determine the orientation of this species.

Figure 3c shows the HREEL spectrum at 77 K after momentarily heating to 230 K. This spectrum is similar to the 185 K spectrum except for the reduction in intensity of the features assigned to the physisorbed pyridine species, indicating that some of this species has desorbed.

Figure 3d shows the HREEL spectrum at 77 K after momentarily heating to 320 K. Except for the 730 cm^{-1} peak, the spectrum is identical to that obtained for pyridine adsorbed at 310 K in the (2√3x3)rect structure, discussed further in the following section, indicating that the same surface species is present. (The pyridine overlayer for the Fig. 3d spectrum, was disordered.) We attribute the 730 cm^{-1} peak to a small amount of the physisorbed pyridine species that has readsorbed during cooling from the residual background pressure of pyridine.

Since the intensities of the HREELS peaks of the chemisorbed species for the 320 K spectrum are similar to those in the 185 and 230 K spectra, we conclude that the physisorbed pyridine species desorbs molecularly during the 295 K molecular desorption peak rather than converting to the chemisorbed pyridine species.

Figure 3e shows the HREEL spectrum after momentarily heating to 445 K. Many of the features that are characteristic of pyridine or α-pyridyl vibrations have disappeared, leading us to conclude that pyridine has completely decomposed by this temperature. The 445 and 820 cm^{-1} peaks and the broad feature centered around 1350 cm^{-1} are similar to those observed for benzene decomposition on Rh(111), where a mixture of C_xH fragments has been proposed to occur [7]. In addition, the 445 K spectrum has other peaks at 330, 1435, and 1575 cm^{-1}, implying the presence of other types of fragments, possibly containing the nitrogen atom from the pyridine molecule.

3.1.3 LEED and HREELS of Pyridine Adsorption at 310 K

For intermediate pyridine exposures (4 to 30 L) with the Rh(111) sample temperature at 310 K, we observed a (2√3x3)rect LEED pattern, which is the same as that observed for benzene on Rh(111) [5] except for the missing of glide plane symmetries. High pyridine exposures caused this pattern to disorder. The notation (2√3x3)rect means that the overlayer orders in a rectangular superlattice and the lattice spacing is 2√3 by 3 times the substrate nearest neighbor distance. Assuming two molecules per unit cell, as was the case for the (2√3x3) rect benzene/Rh(111) structure [5], the pyridine coverage for the (2√3x3) rect structure is one pyridine molecule per six rhodium surface atoms. No other LEED patterns were observed for pyridine adsorbed on Rh(111), even when coadsorbed with CO, which has been found to induce ordering in many overlayers on the Rh(111) surface [5,43].

Figure 4 shows the the HREEL spectrum obtained in the specular direction for the (2√3x3)rect structure of pyridine on the Rh(111) surface. All the features in these spectra decrease in intensity for scattering angles off specular, implying dipole scattering as the scattering mechanism for these features [40]. Also shown is the HREEL spectrum of a low coverage (10% of the (2√3x3)rect coverage) of pyridine on Rh(111). For the (2√3x3)rect structure, Table 1 gives our assignment of the observed HREELS frequencies to the corresponding vibrational frequencies of liquid pyridine. Several of the HREELS frequencies are assigned to more than one pyridine vibrational mode, because of the poorer resolution of HREELS.

The good correspondence between the HREELS frequencies and the vibrational frequencies of liquid pyridine provides strong evidence that the pyridine ring is still intact for chemisorbed pyridine. Recently, Grassian and Muetterties

[13] have studied two osmium cluster compounds - $Os_3(CO)_{11}$ (NC_5H_5), a pyridine complex, and HOs_3 $(CO)_{10}$ (NC_5H_4), an α-pyridyl complex - and have obtained their IR spectra. The vibrational frequencies for these pyridine species correspond well with those observed for pyridine chemisorbed on Rh(111) at 310 K, providing further evidence that the pyridine ring is intact. However, for these cluster compounds, the pyridine and α-pyridyl species have fairly similar vibrational frequencies. With the relatively poor resolution of HREELS, we cannot distinguish from the HREEL spectra alone whether pyridine chemisorbed on Rh(111) at 310 K is a completely intact pyridine species (NC_5H_5) or an α-pyridyl species (NC_5H_4).

We prefer to interpret the HREEL spectra in Fig. 4 as those of an α-pyridyl species on the Rh(111) surface, as the thermal desorption spectra (see section 3.1.1) indicate that partial pyridine dehydrogenation has occurred by 310 K. We also believe that only one species, the α-pyridyl species, is present on the surface at 310 K as 1) the HREELS peaks are fairly narrow rather than being broad or doublet, as would be expected if two surface species were present, and 2) the (2√3x3)rect LEED pattern is sharp with a low background, which is expected if there is only one surface species on the surface.

Another possible interpretation of the 330 K D_2 TDS peak, which cannot be completely ruled out, is that a small fraction of the pyridine molecules lose more than one deuterium or hydrogen atom, while those remaining are completely intact. We think this is unlikely, however, since several features of the decomposed pyridine spectrum (Fig. 3e) - namely, the 330 cm^{-1} peak, the broad feature centered at 1350 cm^{-1}, and the large, sloping background - are absent from the (2√3x3)rect pyridine spectrum (Figure 4b). Also, the HREELS peaks

for decomposed pyridine are substantially broader rather than the peaks present in Figure 4b. For the rest of our discussion of pyridine adsorption on Rh(111), we will assume that only one species is present on the surface for adsorption at 310 K and that this species is an α-pyridyl species, i.e. pyridine that has lost one α-hydrogen and is bonded to the surface through the nitrogen atom and an α-carbon atom.

The α-pyridyl species has also been proposed to form following pyridine adsorption on Pt(111) [13] and Ni(100) [12,27] at 310 K. On these surfaces, evidence for α-pyridyl formation comes from TDS, which shows that partial dehydrogenation occurs by 310 K, from HREELS, which indicates a pyridine-like species tilted perpendicular to the surface, and, for Pt(111), from NEXAFS, which also indicates pyridine-like species tilted perpendicular to the surface. The NEXAFS results are discusssed in more detail below.

Since the metal effectively screens dipole moments oriented parallel to the surface, some information about the orientation of the molecular ring of the α-pyridyl species can be gained by comparing the relative intensities of the HREELS peaks in Figure 4. By comparing the relative intensities of the α-pyridyl vibrational modes oriented parallel to molecular ring (i.e. those corresponding to modes of A_1 or B_1 symmetry in liquid pyridine) to the α-pyridyl modes oriented perpendicular to the molecular ring (i.e., those corresponding to modes of B_2 symmetry in liquid pyridine), we see that the modes oriented perpendicular to the ring are more intense than those oriented parallel to the ring, suggesting that the plane of the molecular ring is oriented more parallel to the surface than perpendicular to the surface. However, several of the in-plane modes (such as the 635 and 1420 cm^{-1} modes in Figure 4b) are fairly intense suggesting that the α-pyridyl species is tilted somewhat away from the surface.

At this point, it is useful to compare pyridine adsorption on Rh(111) at 310 K to pyridine adsorption on Ag(111) and Pt(111), where the orientation of the surface species has been determined by NEXAFS [21,22]. For pyridine adsorption on Ag(111) at 100 K, the tilt angle (i.e. the angle between the ring plane and the surface plane) is 45° ± 5° for low pyridine coverages and 70° ± 5° for high pyridine coverages. For pyridine adsorption on Pt(111), the angle between the ring plane and the surface plane, at 90 K, is 52° ± 6° after annealing to 240 K and is 85° ± 10° after annealing to 320 K. HREEL spectra have also been obtained for pyridine adsorption on Ag(111) and Pt(111). For conditions similar to when NEXAFS finds a large tilt angle (i.e. 70° or 85°) for pyridine adsorption, the vibrational modes oriented parallel to the molecular ring are very intense in the corresponding HREEL spectra. However, for conditions where NEXAFS finds a smaller tilt angle (i.e., 45° or 52°) for pyridine adsorption, the vibrational modes oriented perpendicular to molecular ring are more intense in the HREEL spectra than those oriented parallel to the ring. The intensities of our HREEL spectra for the (2√3x3)rect pyridine Rh(111) structure are more similar to those for pyridine with the smaller tilt angle on Ag(111) and Pt(111) than those with the larger tilt angles. Consequently, we suggest that an angle between 40° and 60° is a reasonable tilt angle for the α-pyridyl species on Rh(111) at 310 K. Fig. 5 shows schematically this orientation of the α-pyridyl species on the surface.

Next, we note that the main difference between the low coverage α-pyridyl spectrum (Fig. 4a) and the high coverage (2√3x3)rect α-pyridyl spectrum (Fig. 4b) is that the in-plane modes are more intense for the high coverage spectrum. This suggests that the tilt angle between the molecular ring and the surface plane increases as the α-pyridyl coverage increases, which might be expected to occur from increased crowding at higher coverages.

Finally, we can gain some insight in the nature of the surface chemical bond of the α-pyridyl species on Rh(111) from the shifts of the observed HREELS frequencies as compared to those of liquid pyridine and to those reported for the $HOs_3(CO)_{10}(NC_5H_4)$, α-pyridyl complex [13]. First, the 750 and 840 cm^{-1} modes of the α-pyridyl/Rh(111) species, which correspond to ν_{25} and ν_{26} of liquid pyridine, are strongly shifted upward from both the liquid pyridine frequencies of 700 and 744 cm^{-1} and the $HOs_3(CO)_{10}(NC_5H_4)$ frequencies of 758, 745, and 740 cm^{-1}. Second, the CH stretching frequencies (~3010 cm^{-1}) are strongly shifted downward from those of liquid pyridine (~3060 cm^{-1}). Similarly large shifts in frequencies have been observed for the same vibrational modes of pyridine chemisorbed on other metal surfaces [12,13,14,15] and for the corresponding vibrational modes of benzene chemisorbed on Rh(111) [3-5] as well as on other metal surfaces [4]. The large magnitude of these frequency shifts relative to the liquid phase frequencies and those of the α-pyridyl cluster complex implies that the α-pyridyl species interacts strongly with the Rh(111) surface. As discussed below, electronic spectroscopy indicates that there is a strong interaction of the π-orbitals of the α-pyridyl species with the surface as well as bonding through the nitrogen and α-carbon atoms. Such an interaction of the π-orbitals with the surface could account for the molecular ring of the α-pyridyl species being incline somewhat toward the surface rather than oriented perpendicular to the surface as observed for the α-pyridyl species on the Pt(111) surface at 300 K [21].

3.2 Benzene Adsorption on Rh(111)

The adsorption of benzene on Rh(111) has been studied extensively, both by workers in our laboratory [1-7] and by researchers in other laboratories [8-10], and has become one of the best characterized aromatic adsorption systems. In this section, we briefly summarize what has been learned about benzene adsorbed on Rh(111) at 310 K. In the following sections, we present new results for benzene adsorbed on Rh(111) obtained by electronic energy loss spectroscopy and optical second-harmonic generation.

HREELS [3-5], TDS [4], and UPS [8,9] all indicate that benzene adsorbs molecularly intact on the Rh(111) surface at 310 K. Further, HREELS [3-5] indicates that benzene forms a strong chemisorption bond with the surface and is oriented at all coverages with its molecular ring parallel to the surface. At saturation benzene coverages, a (2√3x3)rect LEED pattern is observed. The extinction of certain spots in this pattern is also observed, revealing the presence of a glide plane symmetry for this structure. As discussed in Ref. [5], this symmetry requirement, along with the requirement that the molecules must lie flat on the surface, severely restricts the number of possibilities for the arrangement of benzene within the (2√3x3)rect unit cell and led to the conclusion that benzene is centered over bridge sites in this structure.

When CO is coadsorbed with benzene on Rh(111) [5,6], the adsorbed benzene is observed to shift from a bridge-bonded site to one centered over hollow sites. Also, for CO coadsorbed with benzene on Rh(111), two new LEED structures - c(2√3x4)rect and (3x3) - are observed to form. Recently, Van Hove and co-workers have reported dynamical LEED analyses [6] of the c(2√3x4)rect and (3x3) CO + benzene structures; their analyses conclude that

the benzene molecules are distorted from the gas phase structure in a trigonal fashion with C-C bond lengths alternating between those near single and double bonds.

3.3 Electronic Excitations

Figure 6 shows the electronic energy loss spectra for multilayers of benzene and for the ordered benzene and benzene plus CO monolayers on the Rh(111) surface. Figure 7 shows the electronic energy loss spectra for the (2√3x3)rect structure of pyridine on Rh(111). The incident beam energy for these spectra was near 20 eV and the resolution was 15 meV, which is about equal to the width of the figure border for figures 6 and 7. At this beam energy and resolution, the elastic peak intensity was generally too intense to measure accurately due to saturation of our counting electronics. Consequently, we have plotted the absolute intensity of the energy loss features, rather than relative intensities scaled to the intensity of the elastic peak as was done for the vibrational spectra.

The bottom part of Figure 6 shows the electronic EEL spectrum for multilayers of benzene on the Rh(111) surface at 77 K. For the free benzene molecule, the low energy excitations result from the promotion of an electron from the highest occupied π (e_{1g}) orbital to the lowest unoccupied π^* (e_{2u}) orbital. The four-fold degeneracy of this transition is split by electron-electron repulsion to give the $^{1,3}B_{1u}$, $^{1,3}B_{2u}$, and $^{1,3}E_{1u}$ excited states. For gas phase benzene [44], the $^{3}B_{1u} \leftarrow {}^{1}A_{1g}$, $^{1}B_{2u} \leftarrow {}^{1}A_{1g}$, $^{3}E_{1u} \leftarrow {}^{1}A_{1g}$, $^{1}B_{1u} \leftarrow {}^{1}A_{1g}$, and $^{1}E_{1u} \leftarrow {}^{1}A_{1g}$ transitions are observed, respectively, at 3.9, 4.92,

4.85, 6.2, and 6.95 eV. As shown in Table 2, the electronic transitions centered at 4.0, 4.8, 6.2, and 6.8 eV in benzene multilayer spectrum agree well with those for gas phase benzene.

The upper part of Figure 6 shows the electronic EEL spectra for the three ordered structures of benzene and benzene plus CO on the Rh(111) surface at 310 K. The striking feature of these spectra is the absence of prominent π to π^* transitions, which are readily observable for the multilayer spectrum. The absence of the π to π^* transitions in electronic energy loss spectra has been reported for aromatics chemisorbed on other metal surfaces: Pd(111) [19], Pt(111) [45], Ir(111) [16], Ni(111) [18], and Ni(100) [12]. While this absence has been proposed to be due to screening effects [16,45], Avouris and Demuth [46] have pointed out, however, that the ability of these metal surfaces to screen electronic transitions is comparable to that of Ag(111) where the electronic transitions are clearly observed for physisorbed benzene [17]. Instead, Avouris and Demuth have proposed that the absence is directly related to the nature of the strong chemisorption bond that benzene forms with these metal surfaces through its $\pi(e_{1g})$ and $\pi^*(e_{2u})$ orbitals. For benzene chemisorbed on Rh(111), UPS [8,9] shows the presence of many of the occupied orbitals of molecular benzene including the $\pi(e_{1g})$ orbital. However, the $\pi(e_{1g})$ level is broadened and shifted to lower energies by ~1.5 eV relative to the benzene σ orbitals, suggesting that this orbital is strongly involved in the chemisorption bond. The unoccupied $\pi^*(e_{2u})$ should also be broadened in energy due to mixing with surface states, if this orbital is involved in the chemisorption bond. Substantial broadening of the $\pi^*(e_{2u})$ level has been observed by NEXAFS

for benzene chemisorbed on Pt(111) [26]. Consequently, the $\pi(e_{1g})\rightarrow\pi^*(e_{2u})$ excitations would be greatly reduced and difficult to observe. Since only weak transitions are observed in Fig. 6 for chemisorbed benzene, one can infer that the $\pi(e_{1g})$ and $\pi^*(e_{2u})$ orbitals are strongly involved in the chemisorption bond.

The spectra for chemisorbed benzene and benzene plus CO in Figure 6 are shown in comparison to that of the clean Rh(111) surface. For the bare surface, there is a relatively strong excitation centered at 0.7 eV, which we attribute to transitions to rhodium surface states, since it is sensitive to the presence of adsorbates. Also observed is a weak, broad excitation centered at 5.6 eV, which we assign to interband transitions of bulk rhodium [47]. When benzene or benzene plus CO is adsorbed on Rh(111), the 0.7 eV excitation is slightly reduced and shifted in energy and there is now extra intensity in the region extending from 2 eV to 6 eV. As this extra intensity in the 2 eV to 6 eV region does not occur for CO adsorbed alone on Rh(111), we assign it to excitations related to chemisorbed benzene. Similar low energy (1 eV to 5 eV) electronic excitations have been observed for aromatics adsorbed on Ag(111) [17], Ni(100) [12], Pt(111) [19] and Ir(111) [16] and have generally been ascribed to a metal → molecule charge-transfer excitation [46], (i.e., an electron is excited from a metal state to a benzene molecular state). This low energy excitation could also be the weak remains of a $\pi\rightarrow\pi^*$ transition. Interestingly, all the ordered structures of benzene on Rh(111) appear to have the same low energy excitation, even though the shape of the excitation is somewhat different in the different structures.

The spectrum in Figure 7 for α-pyridyl chemisorbed on Rh(111) is similar

to that observed for chemisorbed benzene on Rh(111) in that prominent π to π^* excitations are absent and there is extra intensity in the region from 2 eV to 5 eV. We infer from the absence of prominent π to π^* excitations that the π-orbitals are involved in the bonding of the α-pyridyl species to the Rh(111) surface and the extra intensity as corresponding to charge-transfer excitations or the weak remains of the π to π^* excitations.

3.4 Optical Second-Harmonic Generation (SHG) from Benzene and Pyridine on Rh(111)

We have also monitored benzene and pyridine adsorption on the Rh(111) surface using optical second-harmonic generation. Two incident wavelengths were used, 1.06μm and 532 nm, corresponding to photon energies of 1.17 and 2.34 eV, respectively. So the second-harmonic generated photons have energies of 2.34 and 4.6 eV corresponding to incident wavelengths of 1.06 μm and 532 nm, respectively.

In Figure 8, we show how the SH signal for the Rh(111) surface near room temperature varied as the surface was continuously exposed to benzene. For the 532 nm excitation wavelength, the SH signal is constant for the first 0.68 Langmuirs, then drops from the normalized bare metal value of 1 to the saturation value of 0.44 at about 4.0 Langmuirs of benzene. A (2√3x3)rect LEED pattern was often observed for exposures greater than 4.0 Langmuirs. For the 1.06μm excitation, the SH signal dips slightly to 0.84 of original bare metal value before returning to the bare metal value.

Figure 9 shows the SHG results for pyridine adsorption on the Rh(111) surface. For λ_{ex} = 532 nm, the sample temperature was 275 K, and a steady drop in the SH signal is observed until the SH signal reaches a value 0.24 of

that of the bare metal surface for exposures greater than 4.0 L. For λ_{ex} = 1.06 μm, the sample temperature ranged from 275 K at the start of the pyridine exposure to 235 K at the end of the pyridine exposure; here, the SH signal dips slightly below the bare metal value for intermediate exposures (0-6L) before returning to the bare metal value at high exposures.

The SHG results for benzene and pyridine adsorbed on Rh(111) are quite similar to each other in that, for λ_{ex} = 532 nm, the SH signal drops significantly below the bare metal value and stays there, while, for λ_{ex} = 1.06μm, the SH signal for both molecules drops only slightly before returning to the bare metal value. This similarity can be directly correlated to the similarity between the electronic energy loss spectra of chemisorbed benzene and pyridine (Figs. 6 and 7), as, for both SHG and EELS techniques, the signal is related to the product of the density of states and the dipole matrix elements for the electronic transitions of the surface region [48,49]. Unfortunately, further interpretation of the SHG results is difficult as the detailed nature of the electronic states for chemisorbed benzene and pyridine is not known.

The decrease of the SH signal for λ_{ex} = 532 nm can be correlated with the increase in the intensity of the broad peak at ~4eV with coverage in the electronic ELS spectra for both benzene and pyridine. The increased ELS peak intensity corresponds to an increased contribution from the molecular overlayer to the SH signal which, if opposite in phase, would tend to cancel the SH signal from the bare metal surface, resulting in the observed reduction in the SH signal. For λ_{ex} = 1.06 μm, the resonance effect experienced by $\hbar\omega$ = 1.17 eV from the ~0.8 eV peak in the ELS spectrum should

decrease with increasing coverage, but at $\hbar(2\omega)$ = 2.34 eV the ELS intensity increases with coverage which could enhance the SH signal thereby cancelling the reduction in resonance at 1.17 eV.

Further, we can also correlate the initial plateau observed in the SH signal with λ_{ex}= 532 nm during benzene adsorption with some results reported by Koel et al., [4] who have studied benzene adsorption on Rh(111) as a function of coverage using HREELS, LEED, and TDS. Based on the subtle changes that occur in the HREEL spectra with increasing coverage, Koel et al. concluded that, at low coverages, benzene bonds at one type of adsorption site while, at higher coverages, a second adsorption site becomes occupied. Consequently, the initial plateau would correlate well with the low coverage adsorption site, while the later drop in SH signal for λ_{ex} = 532 nm would correspond to the benzene populating the second adsorption site.

4.6 Conclusions

In this study of pyridine and benzene adsorbed on Rh(111), HREELS has been used to determine both the vibrational and electronic spectra of these adsorbates. At 77 K, multilayers of pyridine are observed with a vibrational spectrum similar to that of liquid pyridine. Between 185 to 230 K, HREELS and TDS indicate that both physisorbed and chemisorbed pyridine species are present on the surface. The physisorbed species desorbs at 295 K, while the chemisorbed species is stable until it decomposes on the surface at 400 K and is identified as an α-pyridyl species.

A (2$\sqrt{3}$x3)rect LEED pattern is observed for both pyridine and benzene adsorption on Rh(111) at 310 K. No ordered structures are observed for CO coadsorbed with pyridine on Rh(111).

Only excitations due to either a charge-transfer band or weak π to π^* transitions are observed in the electronic spectra for benzene and pyridine adsorbed at 310 K. The absence of prominent $\pi \rightarrow \pi^*$ transitions implies that the π-orbitals are strongly involved in the chemisorption bond for these adsorbates.

Optical second-harmonic generation has been used to further monitor benzene and pyridine adsorption on Rh(111). The observed decrease of the SHG signal for λ_{ex}=532 nm is correlated with the electronic spectra. We also find for benzene that the SHG signal is sensitive to the benzene adsorption site.

ACKNOWLEDGEMENTS

We are grateful for helpful discussions with Dr. V.H. Grassian. Also, we thank Drs. J.E. Crowell and T.F. Heinz for their assistance during the second-harmonic generation experiments. This work was supported by the Director, Office of Energy Research, Office of Basic Energy Sciences, Materials Science Division of the U.S. Department of Energy under Contract No. DE-AC03-76SF00098. C.M. Mate gratefully acknowledges a scholarship from the American Vacuum Society; H.W.K. Tom gratefully acknowledges a fellowship from the Hughes Aircraft; X.D. Zhu gratefully acknowledges a fellowship from Dupont.

REFERENCES

1. R.F. Lin, R.J. Koestner, M.A. Van Hove, and G.A. Somorjai, Surface Sci. 134 (1983) 161.
2. M.A. Van Hove, R.F. Lin, and G.A. Somorjai, Phys. Rev. Lett. 51 (1983) 778.
3. B.E. Koel and G.A. Somorjai, J. Electron Spectrosc. 29 (1983) 287.
4. B.E. Koel, J.E. Crowell, C.M. Mate, and G.A. Somorjai, J. Phys. Chem. 88 (1984) 1988; this paper contains a review of vibrational spectroscopy of benzene on metal surfaces.
5. C.M. Mate and G.A. Somorjai, Surface Sci. 160 (1985) 542.
6. M.A. Van Hove, R.F. Lin, and G.A. Somorjai, J. Am. Chem. Soc. 108(1986) 2532; M.A. Van Hove, R.F. Lin, G.S. Blackman, and G.A. Somorjai, Acta Crystallographica B, B43 368 (1987).
7. B.E. Koel, J.E. Crowell, B.E. Bent, C.M. Mate, and G.A. Somorjai, J. Phys. Chem. 90 (1986) 2949.
8. M. Neumann, J.U. Mack, E. Bertel, and F.P. Netzer, Sur. Sci. 155(1985) 629.
9. E. Bertel, G. Rosina, and F.P. Netzer, Surface Sci. 172 (1986) L515.
10. E.L. Garfunkel, C. Minot, A. Gavezzotti, and M. Simonetta, Surface Sci. 167 (1986) 177.
11. J.E. Demuth, K. Christmann, and P.N. Sanda, Chem. Phys. Lett. 76 (1980) 201.
12. N.J. DiNardo, Ph. Avouris, and J.E. Demuth, J. Chem. Phys. 81 (1984) 2169.
13. V.H. Grassian and E.L. Muetterties, J. Phys. Chem., 90(1986) 5900;
14. V.H. Grassian and E.L. Muetterties, J. Phys. Chem., 91(1987) 389;
15. G.D. Waddill and L.L. Kesmodel, Chem. Phys. Letters, 128(1986) 208.
16. F.P. Netzer, E. Bertel and J.A.D. Mathew, Surface Sci. 92 (1980) 43.
17. Ph. Avouris and J.E. Demuth, J. Chem. Phys. 75 (1981) 4783.

18. H.J. Robota, P.M. Whitmore and C.B. Harris, J. Chem. Phys. 76 (1982) 1692.

19. F.P. Netzer and J.U. Mack, J. Chem. Phys. 79 (1983) 1017.

20. Ph. Avouris, N.J. DiNardo, and J.E. Demuth, J. Chem. Phys. 80 (1984) 491.

21. A.L. Johnson, E.L. Muetterties, J. Stohr, and F. Sette, J. Phys. Chem. 89 (1985) 4071.

22. M. Bader, J. Hasse, K.-H. Frank, A. Puschmann, and A. Otto, Phys. Rev. Lett. 56 (1981) 1921.

23. B.J. Bandy, D.R. Lloyd, and N.V. Richardson, Surface Sci. 89 (1979) 344.

24. J.U. Mack, E. Bertel, and F.P. Netzer, Surface Sci. 159 (1985) 265.

25. F.P. Netzer and J.U. Mack, Cem. Phys. Lett. 95 (1983) 492.

26. J.A. Horsley, J. Stöhr, A.P. Hitchcock, D.C. Newbury, A.L. Johnson, and F. Sette, J. Chem. Phys. 83(1985) 6099.

27. R.M. Wexler, M.-C. Tsai, C.M. Friend, and E.L. Muetterties, J. Am. Chem. Soc. 104 (1982) 2034.

28. G.D. Waddill and L.L. Kesmodel, Phys. Rev. B31 (1985) 4940.

29. J.C. Bertolini and J. Rousseau, Surface Sci. 89 (1979) 467.

30. J.C. Bertolini, J. Massaradier, and B. Tardy, J. Chem. Phys. 78 (1981) 939.

31. S. Lehwald, H. Ibach and J.E. Demuth, Surface Sci. 78 (1978) 577.

32. J. Massardier, B. Tardy, M. Abon and J.C. Bertolini, Surface Sci. 126 (1983) 154.

33. G.L. Nyberg, S.R. Bare, P. Hoffmann, D.A. King and M. Surman, Appl. Surf. Sci. 22/23 (1985) 392; M. Surman, S.R. Bare, P. Hofmann and D.A. King, Surface Sci. 179 (1987) 243.

34. F.G. Ciapetta and D.N. Wallace, Catal. Rev. 5 (1972) 67.

35. D.H. Buckeley, Surface Effects in Adhesion, Friction, Wear and Lubrication, Elsevier, Amsterdam, 1981, p. 544.

36 H. Froitzheim, H. Ibach and S. Lehwald, Rev. Sci. Instr. 46(1975) 1325.

37. P.A. Redhead, Vacuum 12 (1962) 203.

38. J.P. McCullough, D.R. Douslin, J.F. Messerly, I.A. Hossenlopp, T.C. Kincheloe and G. Waddington, J. Am. Chem. Soc. 79 (1957) 4289.

39. J.T. Yates, Jr., P.A. Thiel, and W.H. Weinberg, Surface Sci. 84 (1979) 427.

40. H. Ibach and D.L. Mills, Electron Energy Loss Spectroscopy and Surface Vibrations, Academic Press, New York, 1982, pp. 201-4.

41. R. Azria and G.J. Schulz, J. Chem. Phys., 62(1975) 573.

42. K.B. Wiberg, V.A. Walters, K.N. Wong, and S.D. Colson, J. Phys. Chem. 88 (1984) 6067.

43. C.M. Mate, B.E. Bent and G.A. Somorjai, J. Electron Spectrosc., 39(1986) 205.

44. J.P. Doering, J. Chem. Phys. 67 (1977) 4065.

45. F.P. Netzer and J.A.D. Mathew, Solid State Commun. 29 (1979) 209.

46. Ph. Avouris and J.E. Demuth, Surface Sci. 158 (1985) 21.

47. J.H. Weaver, C.G. Olson, and D.W. Lynch, Phys. Rev. B15 (1977) 4115.

48. Y.R. Shen, The Principles of Nonlinear Optics, Wiley, New York, 1984, pp. 17.

49. H. Ibach and D.L. Mills, p. 97.

Table 1. Assignment of observed vibrational frequencies (cm^{-1}) for pyridine adsorbed on Rh(111).

(2√3x3)rect Pyridine/Rh(111) $NC_5H_5(NC_5D_5)$	Multilayer Pyridine/Rh(111)	Liquid Phase Frequencies [42] $NC_5H_5(NC_5D_5)$	Liquid Phase Mode No. (Symm. Representation) [42]
345 (345)		--	pyridine-Rh
465 (425)	410	403 (367)	27 (B_2)
635 (635)		601 (579)	10 (A_1)
		652 (625)	19 (B_1)
750 (565)		700 (526)	26 (B_2)
	730		
840 (725)		744 (631)	25 (B_2)
		936 (765)	24 (B_2)
		991 (963)	9 (A_1)
1025 (825)	1000	1007 (828)	23 (B_2)
(990)		1032 (1014)	8 (A_1)
		1072 (823)	7 (A_1)
		1079 (835)	18 (B_1)
1130 (825)		1143 (856)	17 (B_1)
		1218 (882)	6 (A_1)
1240 (1240)	1220	1227 (1226)	16 (B_1)
		1362 (1046)	15 (B_1)
1420 (1325)	1450	1442 (1303)	14 (B_1)
		1483 (1340)	5 (A_1)
1550 (1485)	1590	1581 (1546)	13 (B_1)
		1583 (1554)	4 (A_1)
		3030 (2268)	3 (A_1)
3010 (2240)	3060	3042 (2256)	12 (B_1)
		3087 (2289)	11 (B_1)
		3094 (2302)	1 (A_1)

Table 2. Electronic excitation energies (in eV) for gas phase benzene and multilayers of benzene on Rh(111).

Transitions	Gas phase [44]	Benzene multilayers on Rh(111)
$^3B_{1u} \leftarrow {}^1A_{1g}$	3.9	4.0
$^1B_{2u} \leftarrow {}^1A_{1g}$	4.92	4.8
$^3E_{1u} \leftarrow {}^1A_{1g}$	4.85	4.8
$^1B_{1u} \leftarrow {}^1A_{1g}$	6.2	6.2
$^1E_{1u} \leftarrow {}^1A_{1g}$	6.95	6.8

FIGURE CAPTIONS

Fig. 1 Schematic of the reaction of pyridine with various metal surfaces as reported in the literature(11-15, 19, 21-25, 27, 33) and in this paper for Rh(111). The tilt angles were measured by NEXAFS or estimated from HREELS peak intensities and correspond to the angle between the plane of the pyridine ring and the surface plane.

Fig. 2 Thermal desorption spectra of NC_5H_5 (Amu 79) and D_2 (Amu 4) following a large exposure (~50 L) to NC_5H_5 or NC_5D_5 on Rh(111) at 80 K.

Fig. 3 Vibrational spectra obtained by HREELS in the specular direction for multilayers of pyridine on Rh(111) and after momentarily heating to the indicated temperatures. The spectra were taken with a sample temperature of 77 K for spectra a, b, c, and d, and of 310 K for spectra e.

Fig. 4 Vibrational spectra for pyridine adsorbed on Rh(111) at 310 K.

Fig. 5 Proposed bonding and orientation of the α-pyridyl species on the Rh(111) surface.

Fig. 6 Electronic energy loss spectra for benzene and benzene plus CO on Rh(111). The dashed curves show the spectrum of the clean Rh(111) surface for comparison. The resolution is 15 meV.

Fig. 7 Electronic energy loss spectrum for the $(2\sqrt{3}x3)$rect structure of pyridine on Rh(111). The dashed curve shows the spectrum of the clean Rh(111) surface for comparison. The resolution is 15 meV.

Fig. 8 Second-harmonic signal from the Rh(111) surface during exposure to benzene.

Fig. 9 Second-harmonic signal from the Rh(111) surface during exposure to pyridine.

α- pyridyl on Rh(111)

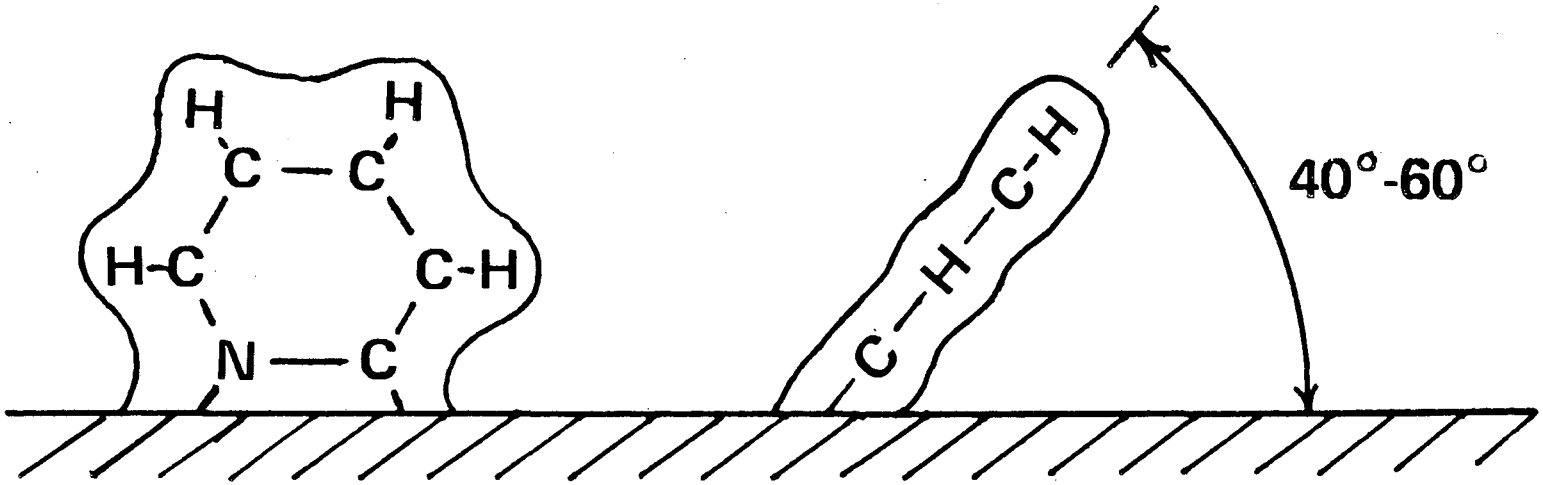

XBL 875-2341

Fig. 1

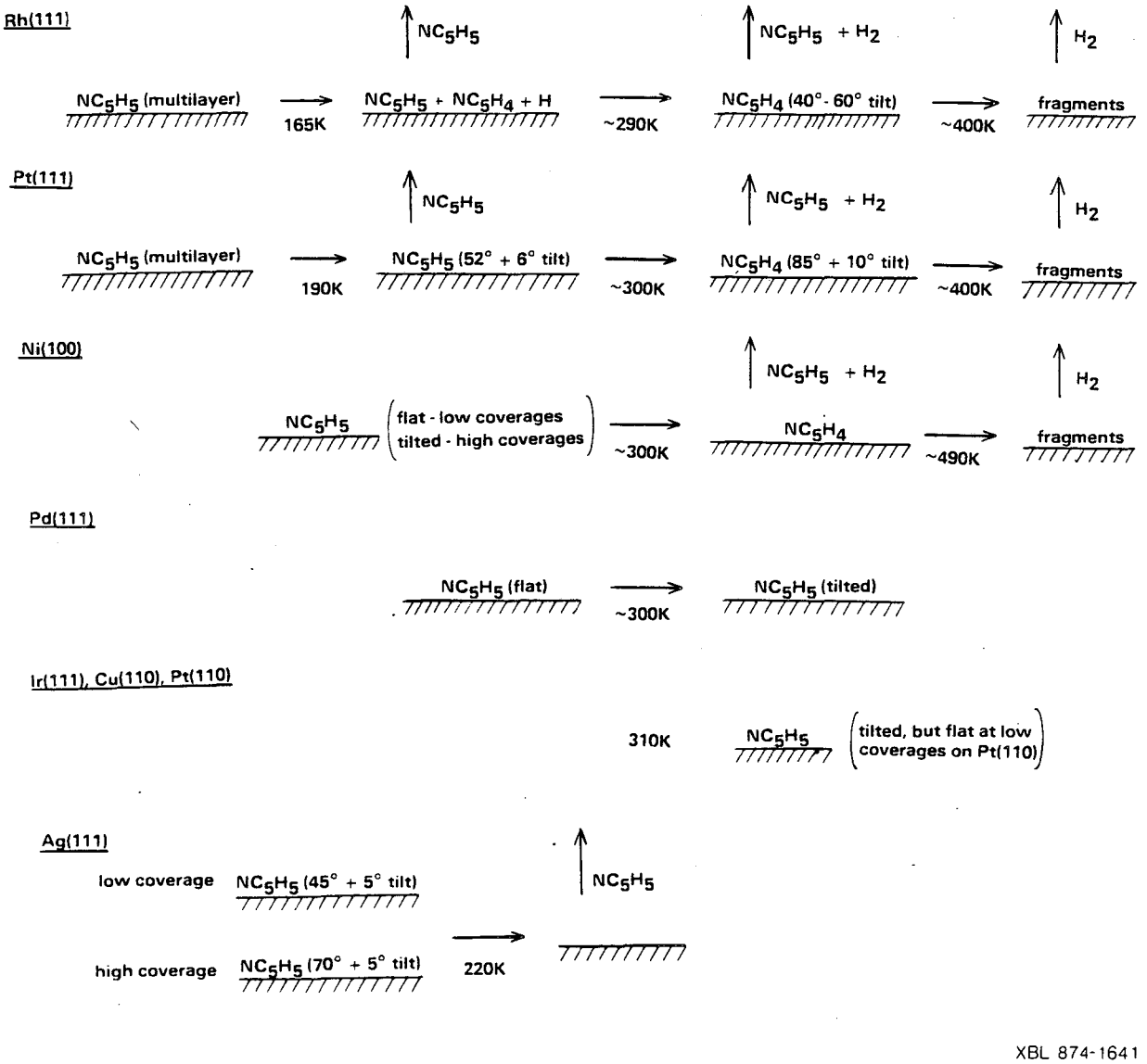

XBL 874-1641

Fig. 2

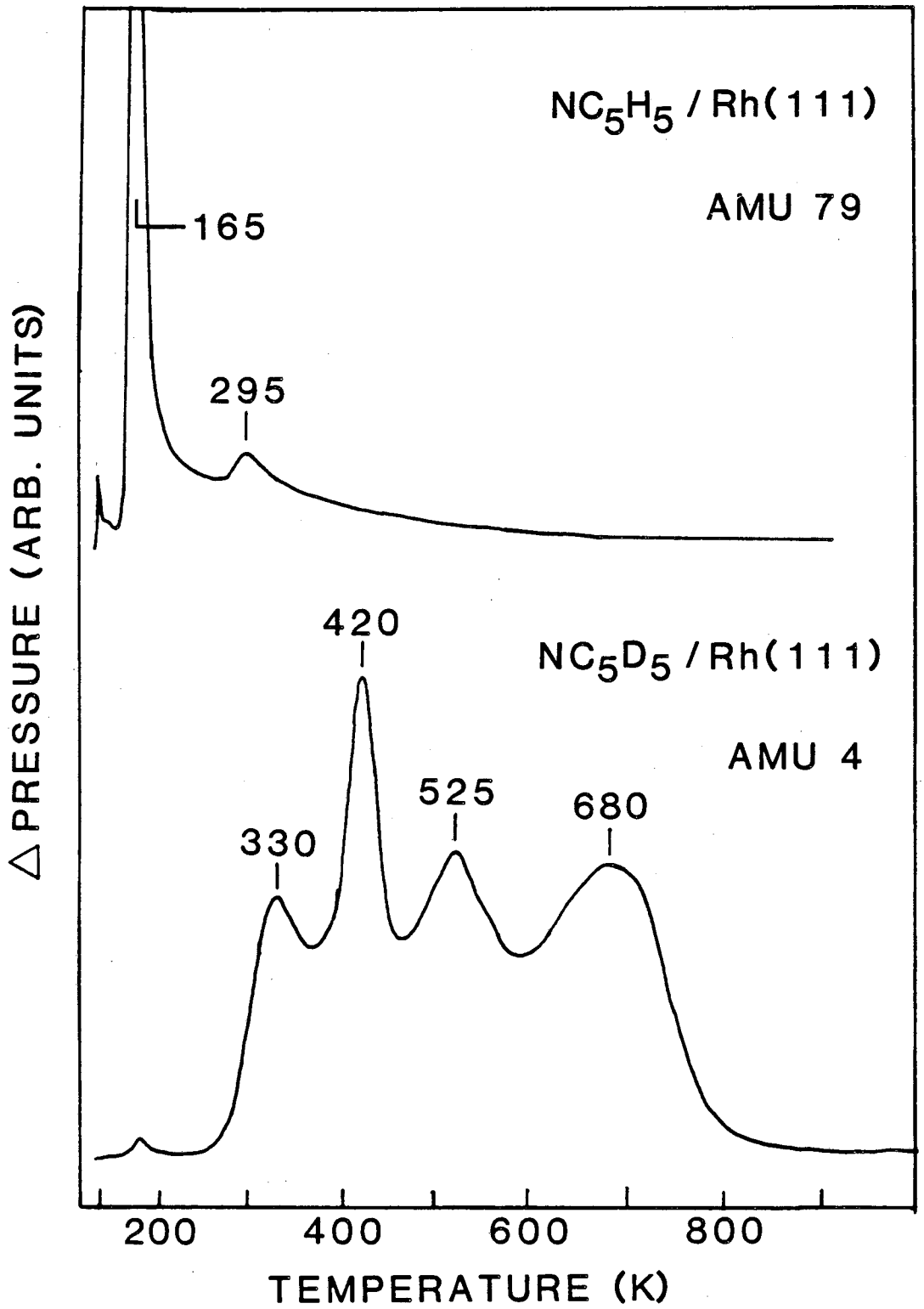

XBL 869-3421

Fig. 3

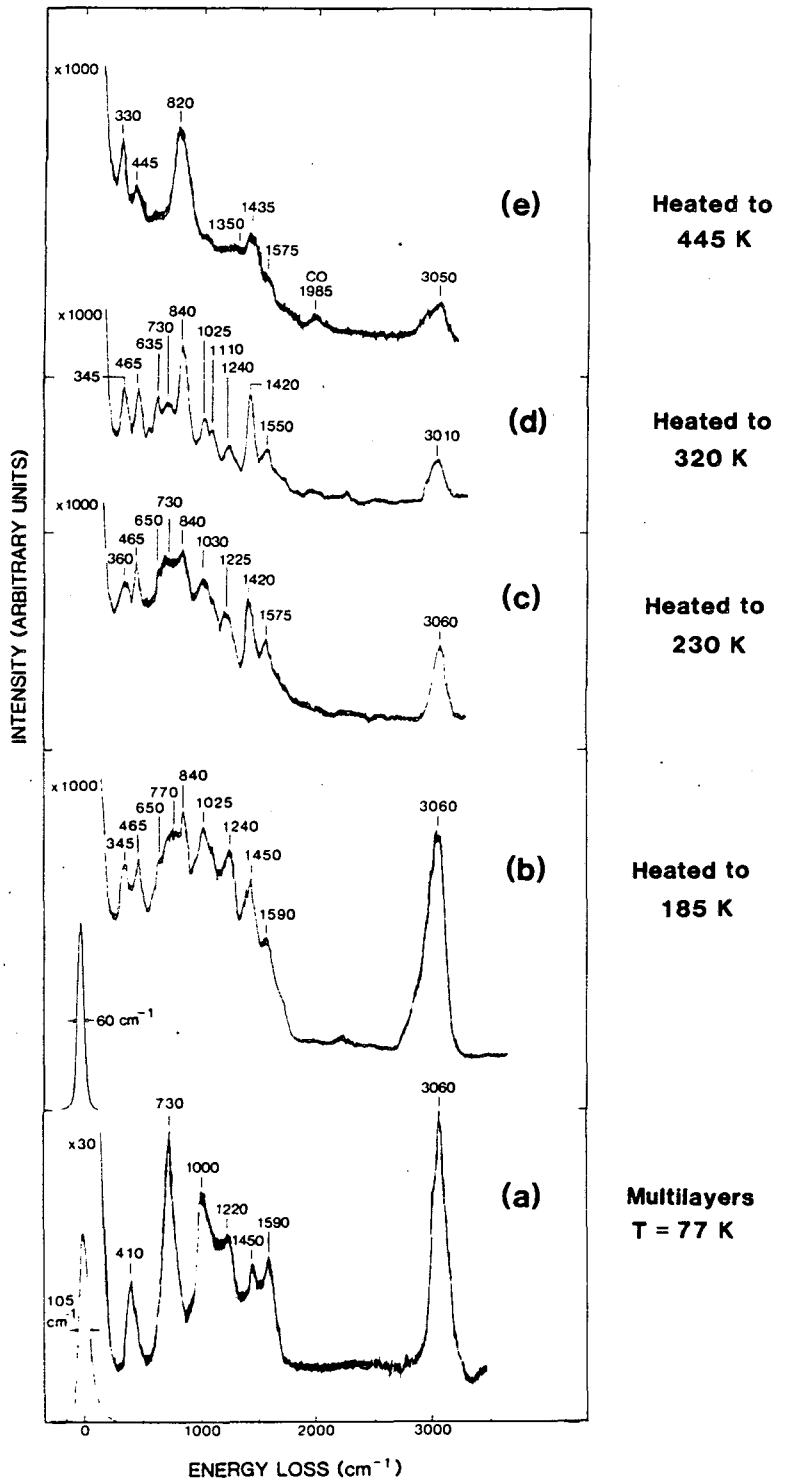

XBL 869-3436

Fig. 4

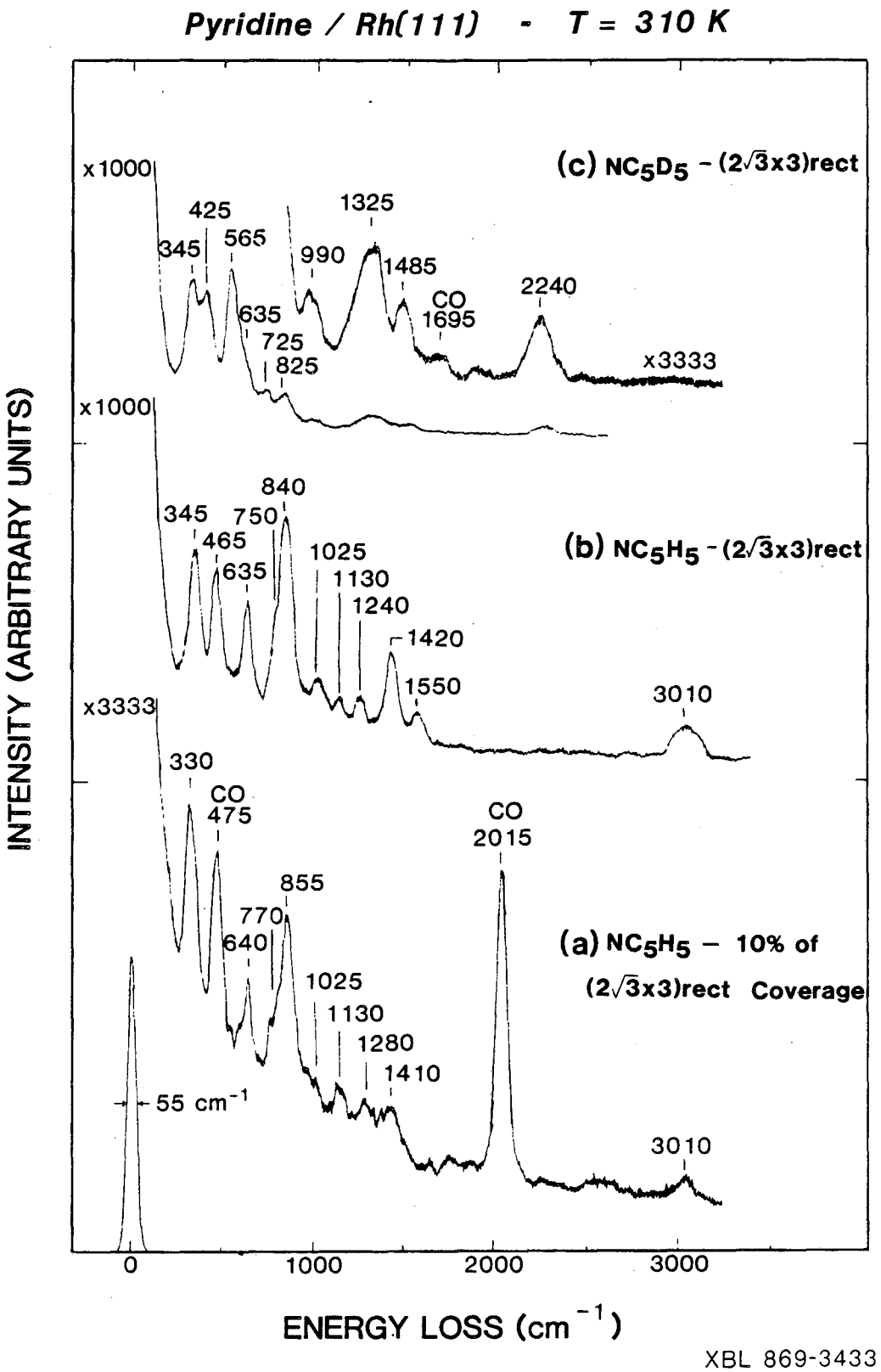

XBL 869-3433

Fig. 5

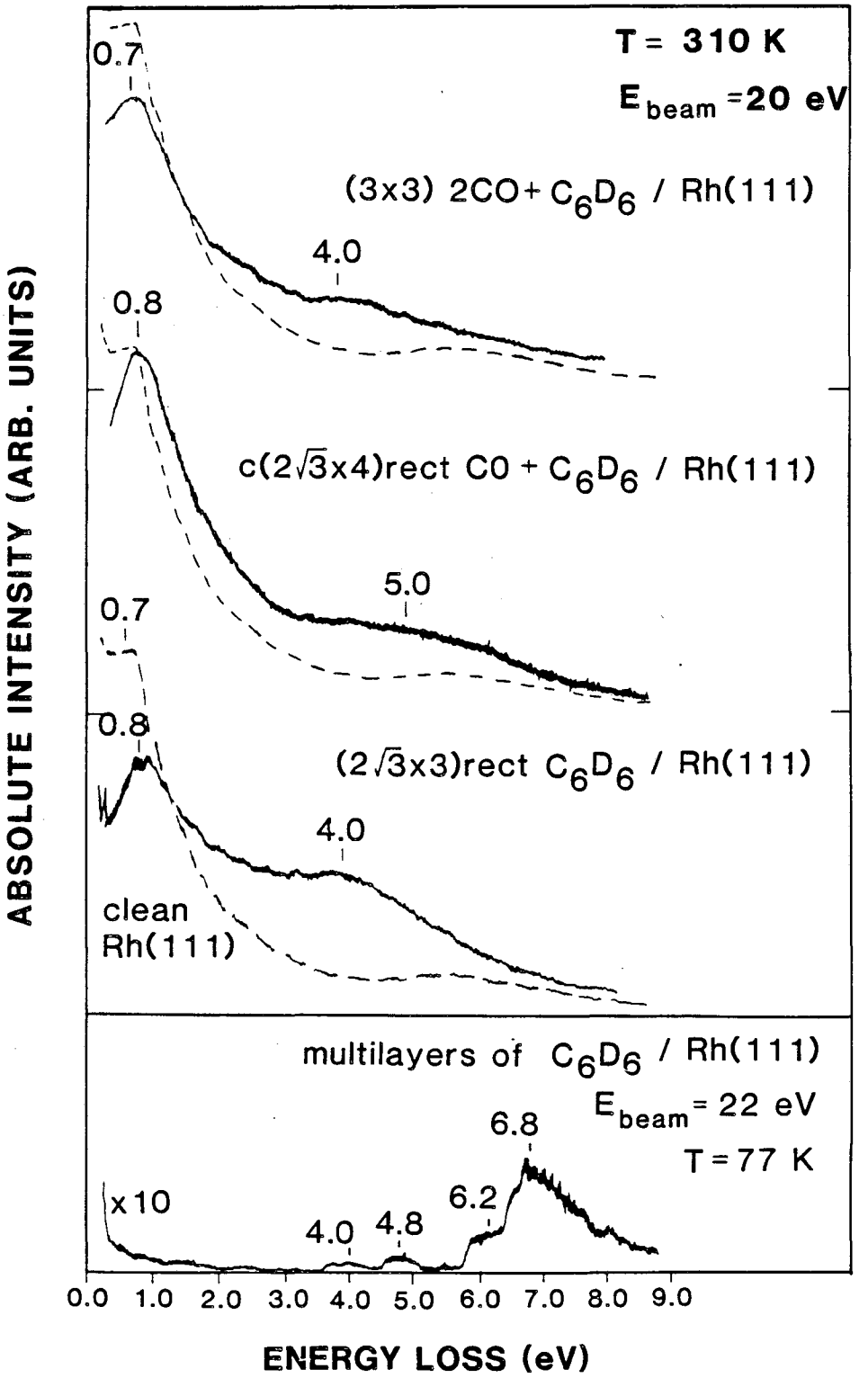

XBL 869-3423

Fig. 6

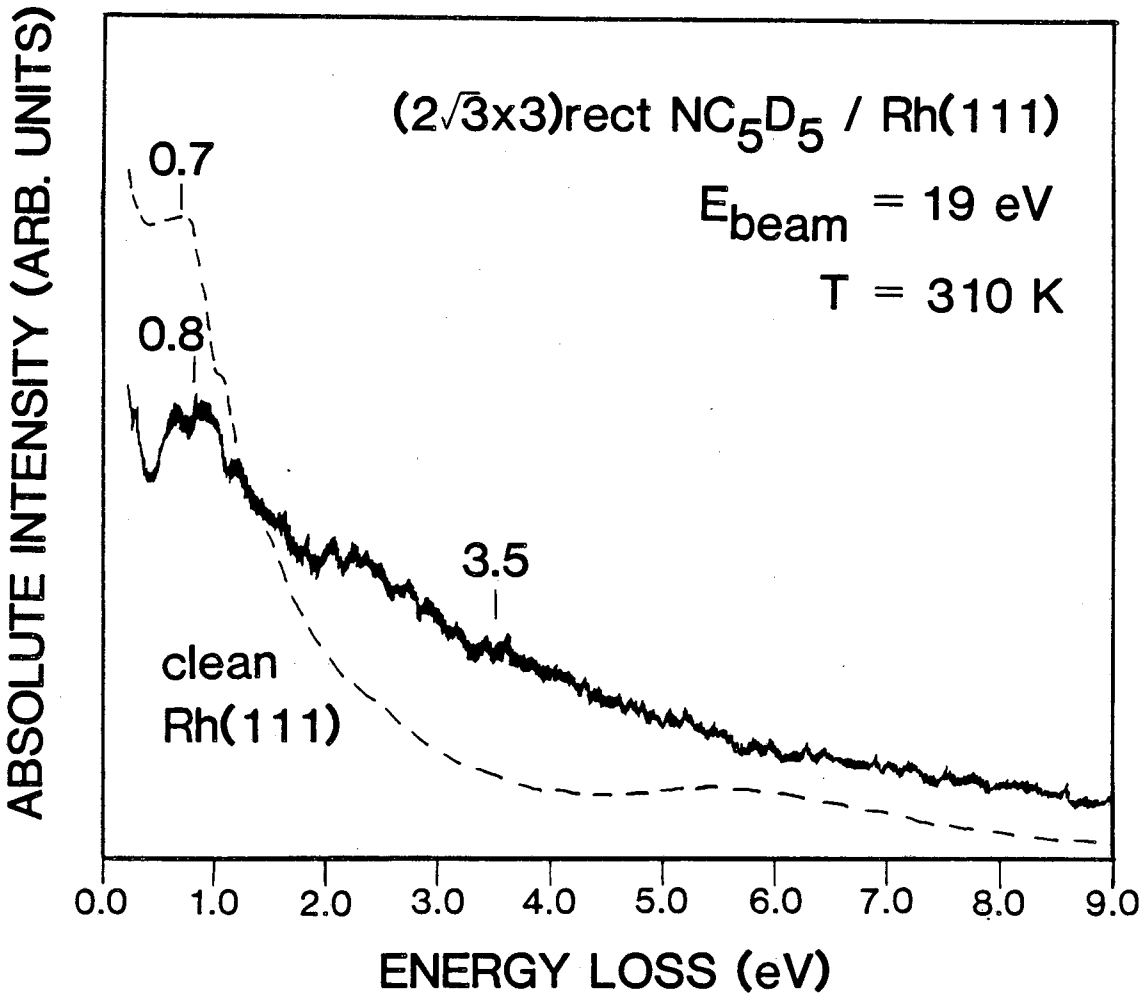

XBL 869-3422

Fig. 7

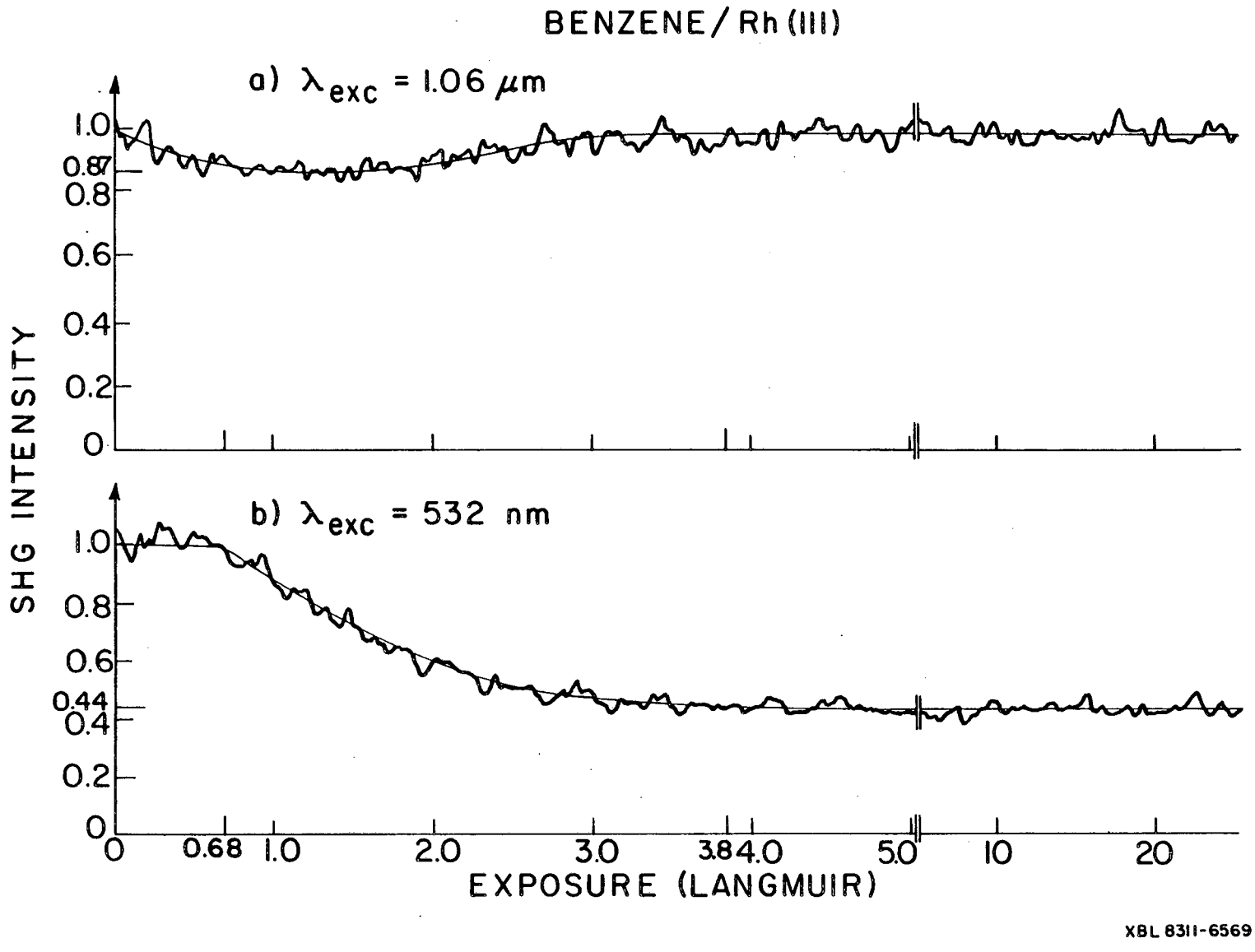
BENZENE / Rh (III)
a) λ_{exc} = 1.06 μm
b) λ_{exc} = 532 nm
SHG INTENSITY
1.0
0.87
0.8
0.6
0.4
0.2
0
1.0
0.8
0.6
0.44
0.4
0.2
0
0
0.68
1.0
2.0
3.0
3.8
4.0
5.0
10
20
EXPOSURE (LANGMUIR)
XBL 8311-6569

Fig. 8

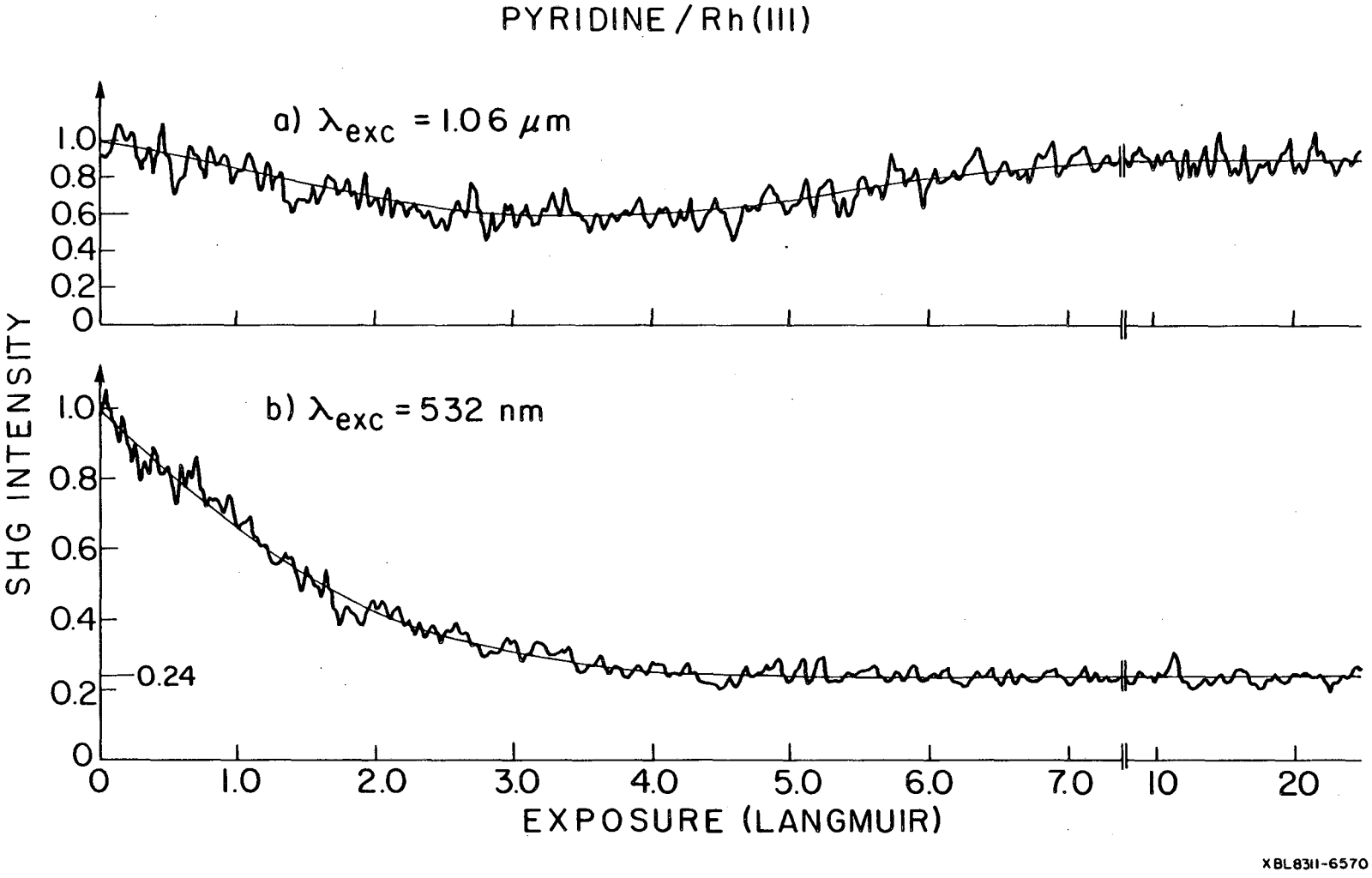
PYRIDINE / Rh(III)
a) λ_{exc} = 1.06 μm
b) λ_{exc} = 532 nm
SHG INTENSITY
1.0
0.8
0.6
0.4
0.2
0
0.24
0
1.0
2.0
3.0
4.0
5.0
6.0
7.0
10
20
EXPOSURE (LANGMUIR)
XBL8311-6570

Fig. 9

LAWRENCE BERKELEY LABORATORY
TECHNICAL INFORMATION DEPARTMENT
UNIVERSITY OF CALIFORNIA
BERKELEY, CALIFORNIA 94720